
Since January 2020 Elsevier has created a COVID-19 resource centre with free information in English and Mandarin on the novel coronavirus COVID-19. The COVID-19 resource centre is hosted on Elsevier Connect, the company's public news and information website.

CHAPTER ONE

# The viral replication organelles within cells studied by electron microscopy

**Martin Sachse[a,*], Isabel Fernández de Castro[b], Raquel Tenorio[b], Cristina Risco[b,*]**

[a]Unité Technologie et service BioImagerie Ultrastructurale, Institut Pasteur, Paris, France
[b]Cell Structure Laboratory, National Center for Biotechnology, CSIC, Madrid, Spain
*Corresponding authors: e-mail address: martin.sachse@pasteur.fr; crisco@cnb.csic.es

## Contents



## Abstract

Transmission electron microscopy (TEM) has been crucial to study viral infections. As a result of recent advances in light and electron microscopy, we are starting to be aware of the variety of structures that viruses assemble inside cells. Viruses often remodel cellular compartments to build their replication factories. Remarkably, viruses are also able to induce new membranes and new organelles. Here we revise the most relevant imaging technologies to study the biogenesis of viral replication organelles. Live cell microscopy, correlative light and electron microscopy, cryo-TEM, and three-dimensional imaging methods are unveiling how viruses manipulate cell organization. In particular, methods for molecular mapping in situ in two and three dimensions are revealing how macromolecular complexes build functional replication complexes inside infected cells. The combination of all these imaging approaches is uncovering the viral life cycle events with a detail never seen before.

*Advances in Virus Research*, Volume 105
ISSN 0065-3527
https://doi.org/10.1016/bs.aivir.2019.07.005

## Abbreviations

| | |
|---|---|
| **CEMOVIS** | cryo-electron microscopy of vitreous sections |
| **CLEM** | correlative light and electron microscopy |
| **EM** | electron microscopy |
| **ET** | electron tomography |
| **FIB** | focused-ion beam |
| **FS** | freeze-substitution |
| **GFP** | green fluorescence protein |
| **HPF** | high-pressure freezing |
| **LM** | light microscopy |
| **METTEM** | metal-tagging TEM |
| **MT** | metallothionein |
| **RO** | replication organelle |
| **RT** | room temperature |
| **SEM** | scanning electron microscopy |
| **STEM** | scanning-transmission electron microscopy |
| **3D** | three-dimensional |
| **TEM** | transmission electron microscopy |
| **2D** | two-dimensional |
| **VF** | virus factory |
| **VRC** | viral replication complex |
| **vRNP** | viral ribonucleoprotein |

## Virus names

| | |
|---|---|
| **BUNV** | Bunyamwera virus |
| **DENV** | dengue virus |
| **FHV** | flock house virus |
| **FMDV** | foot-and-mouth disease virus |
| **HCV** | hepatitis C virus |
| **HIV** | human immunodeficiency virus |
| **SARS CoV** | severe acute respiratory syndrome coronavirus |
| **SFV** | Semliki forest virus |
| **TBSV** | tomato bushy stunt virus |
| **VV** | vaccinia virus |

## 1. Introduction

The common hallmark of all viruses is their dependency on a host cell to infect and multiply. During this cycle the virus utilizes and transforms the machinery of the cell for the biosynthesis of the own genetic material, proteins, and lipids. This can lead to vast reorganization in the subcellular

organization inside the cell (Risco et al., 2014; Romero-Brey and Bartenschlager, 2014). The size of most viruses is beyond the resolution limit of optical microscopy, and only electron microscopy (EM) provides the resolution required to study viruses and their life cycles (Pelchen-Matthews and Marsh, 2007).

The technical specifications of an electron microscope are, however, only one part of the equation to deliver insight into the viral life cycle within the host cell. The first obstacle comes from the dynamic nature of the virus cycle. Infection, replication, virus particle morphogenesis and egress are different, consecutive steps. But in contrast to optical microscopy, EM does not permit the observation of the same object over time. This aspect can be solved with the study of different samples after finding the right time post-infection for each step. Next to the dynamics of these different steps during viral infection, another challenge arises from their topology: only entry and release of the viral particle take place at the surface of the host cell. All other steps utilize machineries inside the cell and their study requires the analysis of the morphology of the cell interior. For this reason, transmission electron microscopy (TEM) combined with thin sections of infected cells has been for a long time the standard approach to study the intracellular aspects of virus life cycles. However, the morphology of a cell is three-dimensional and thus random thin sections provide a limited view. As pointed out more than 60 years ago, the impact of EM for the morphological analysis of viruses depends highly on technological progress on sample preparation (Hillier, 1950). Since this time, sample preparation as well as the sensitivity of electron microscopes and their detectors has evolved to a great extent and different approaches for tomography were developed to study samples in 3D. But the key point raised at that time has remained: each sample preparation/imaging technique produces artifacts and it is important to be aware of them and be critical about the amount of information that can be extracted. Simultaneously with the technological development, our knowledge about the life cycle of viruses has increased, and the diversity of the questions addressed has increased concomitantly. It is often required to combine different approaches to answer the question at hand. Therefore, this review will focus on the different preparation and imaging techniques that are used to visualize the cell biology of viral infections (Fig. 1). We will discuss the technological basis of the different approaches and the findings they made possible. In particular, we will focus on the characterization of virus factories and virus replication organelles. Viruses express their fundamental biological properties during the intracellular stage of their life cycle,

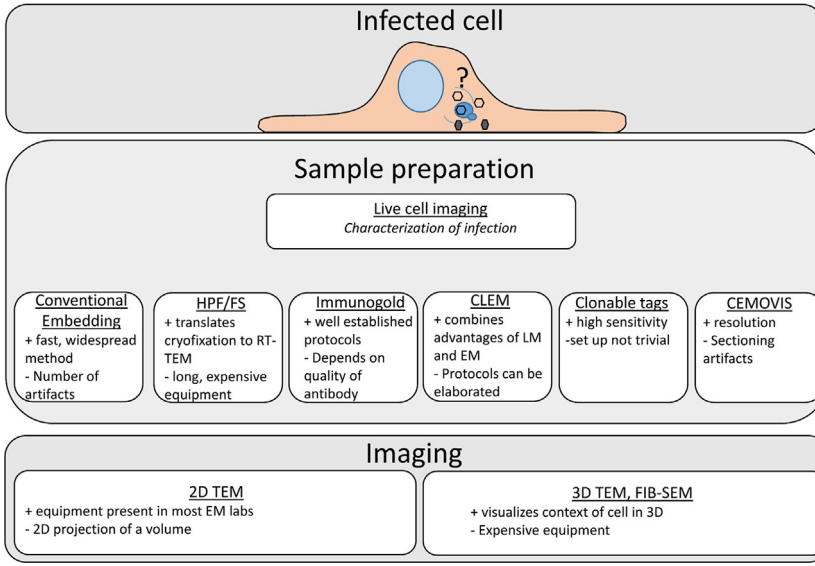


**Fig. 1** Scheme summarizing the different approaches for sample preparation and imaging, which are discussed in this review. Life cell imaging provides the best approach to characterize the dynamics of infection and the assembly of replication organelles. Based on these data the EM experiments can be designed. The choice of sample preparation protocols will depend on the questions of interest and the available possibilities. Main advantages (+) and limitations (−) of each method are indicated.

which in most cases takes place within virus factories (Fernández de Castro et al., 2013). Viral factories (VF) are intracellular membranous compartments harboring viral replication organelles (RO) that contain viral replication complexes (VRC) and the sites of virus particle assembly (Harak and Lohmann, 2015; Novoa et al., 2005). VRCs are often located in single-membrane vesicles known as spherules, but also in double-membrane vesicles (DMVs), flat membranes and cubic/convoluted membranes (CM) (Fernández de Castro et al., 2013). To build these neoorganelles, viruses manipulate lipid synthesis and flows to create platforms with particular lipid composition and biophysical properties that facilitate viral genome replication (Altan-Bonnet, 2017; Fernández de Castro et al., 2016; Fernández-Oliva et al., 2019). Due to their complex composition and functions, virus factories could be contemplated as the living state of viruses (Fridmann-Sirkis et al., 2016). Two main pathways have been identified so far as being responsible for viral factory biogenesis: aggresome formation for DNA viruses and autophagy for RNA viruses (Abernathy et al., 2019; Jackson et al., 2005; Kajitani et al., 2013; Wileman, 2007).

Mitochondria and cytoskeleton elements are often found around replication organelles building a large structure that usually transforms the whole cell content (Fernández de Castro et al., 2013). Viral factories are dynamic structures that change over time and maintain communication with intracellular transport pathways such as endocytosis and exocytosis, which are necessary in order to incorporate essential factors into the factories and to facilitate virus egress (Altan-Bonnet, 2017; Fontana et al., 2010). Some viruses build factories inside the nucleus (Erickson et al., 2012) but most of the structural information available to date comes from cytoplasmic viral factories (Risco et al., 2014).

## 2. Live cell imaging

Despite the focus on EM of this review we must highlight light microscopy (LM) as a great ally of electron microscopists. This is due to the ability of LM to characterize dynamic changes in the cell associated to viral infection, albeit with less resolution but with shorter times for sample preparation. Furthermore, new advances in fluorescent probes and LM methods are providing new insights into the cell biology of viruses. Very interesting recent reviews deal with light microscopy of viral infections (Alonas et al., 2016; Dirk et al., 2016; Hanne et al., 2016; Witte et al., 2018). However, microscopy of fixed cells provides static views of complex, dynamic events. To study multi-step processes such as a virus infection, time-course assays are useful and provide data that we try to organize sequentially. Nevertheless, during viral infections what we perceive as a logical sequence of events might not correspond to reality, and many findings would have never been uncovered without dynamic, real time, live cell microscopy. Live-cell imaging of viral infections has been mainly focused on processes of entry and release of viral particles (Baktash et al., 2018; Francis and Melikyan, 2018; Jouvenet et al., 2008) but has shown great potential to study all steps of the virus replication cycle (Campbell and Hope, 2008). Live cell microscopy can also reveal a heterogeneous response of cells to infection (Movie 1 in the online version at https://doi.org/10.1016/bs.aivir.2019.07.005, Fig. 2). When mammalian cells infected with a fluorescent bunyavirus (Shi et al., 2010) are studied by live cell imaging, it can be observed that some cells rapidly build a virus factory and produce many progeny viruses (Fig. 2, cell 1), a few cells die soon (Fig. 2, cell 2) and some others apparently do not get infected (Fig. 2, cell 3). Indeed, some cells receive the fluorescent virus and pass it to neighboring cells while remaining

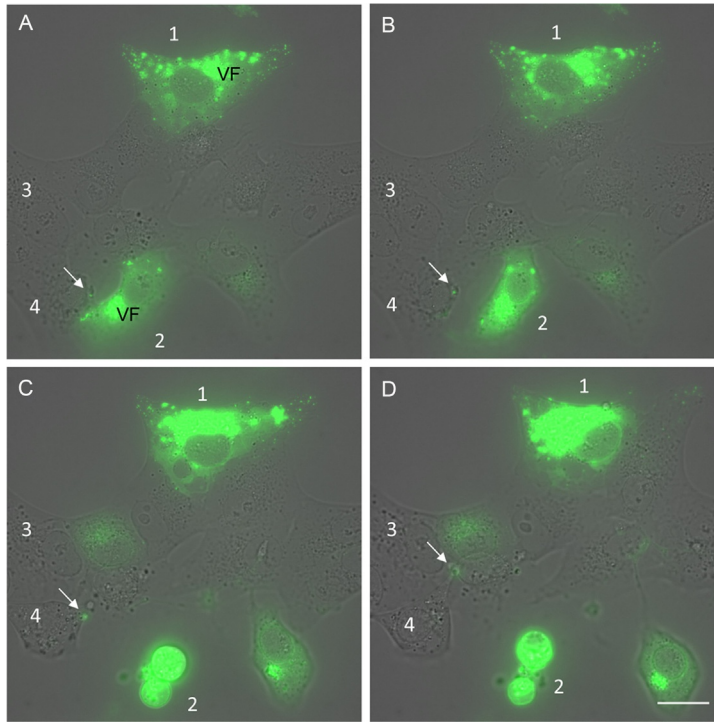


**Fig. 2** Snapshots from Movie 1 in the online version at https://doi.org/10.1016/bs.aivir.2019.07.005 showing different stages of viral factory biogenesis and a heterogeneous response of cells to the virus. BHK-21 cells infected with the fluorescent bunyavirus eGFP-Gc-BUNV at a multiplicity of infection (MOI) of 5 PFU/cell, were transferred to a TCS-SP5 microscope (Leica Microsystems) and images recorded every 15 min from 1 h post-infection (hpi) to 18 hpi. Images correspond to 8 h and 15 min post-infection (A), 8 h and 45 min pi (B), 13 h and 45 min pi (C), and 15 h and 30 min pi (D). In cell #1, a large viral factory (VF) assembles and grows over time. Cell #2 assembles a VF and dies soon. Cell #3 remains apparently non-infected and cell #4 receives fluorescent viruses (arrows in A–C), passes them to another cell (arrow in D) and remains non-infected. Scale bar: 25 μm. Sanz-Sánchez and Risco, unpublished results.

apparently non-infected (Fig. 2, cell 4). These findings demonstrate that cells in the cultured cell monolayer are not identical and respond to virus infection heterogeneously.

An interesting case was reported in a study of mosquito cells infected with an arbovirus (López-Montero and Risco, 2011). Video-microscopy showed that all infected cells went through three different stages of infection, early, acute and persistent, something that can be fully appreciated only when following each single cell in real time (López-Montero and Risco, 2011). Live-cell imaging has been used to study the biogenesis, dynamics

and trafficking of viral replicative structures. Remarkably, these studies have shown that unrelated viruses such as Vaccinia Virus, Hepatitis C Virus, rotaviruses and the mouse hepatitis coronavirus, assemble small replication organelles that move through the cytoplasm in a microtubule-dependent manner, together with larger replication platforms that are rather immobile (Baktash and Randall, 2019; Eichwald et al., 2012; Eyre et al., 2014; Hagemeijer et al., 2010; Schramm et al., 2006; Wölk et al., 2008). Live-cell imaging has also shown the transformation of cell compartments induced by viruses to build their replication organelles. This is the case of the enterovirus coxsackievirus B3 that disassembles the Golgi complex (Van der Schaar et al., 2016) or the human reovirus that remodels the endoplasmic reticulum to build viral inclusions (Tenorio et al., 2018). New probes for imaging viral RNA will be powerful tools to study viral replication and assembly in live cells (Alonas et al., 2016).

For obtaining reproducible results by live cell imaging, the experiment must be carefully designed and adequate controls have to be included. Before starting, a number of important factors should be taken into account. Fluorescent probes must be compatible with in vivo conditions (Galas et al., 2018). Cells have to be grown on special plates with a clear bottom made of plastic or glass and plated with an appropriate confluence, usually 70% or less. A previous time-course study by confocal microscopy of fixed cells is important to determine the best time post-infection for launching the live cell imaging recording. To limit potential effects caused by phototoxicity, the right choice of fluorescent proteins, light intensity, exposure time and time interval between frame acquisitions will be critical (Magidson and Khodjakov, 2013; Icha et al., 2017).

For a detailed understanding of events, either expected or rare, live cell imaging is a powerful partner of EM through the methods we know as Correlative Light and Electron Microscopy (CLEM) (see Section 4).

## 3. General aspects of sample preparation for transmission electron microscopy

For a morphological study by EM the goal should be to preserve the samples as close as possible to the condition of interest and keep all cellular components in place. The electron microscope adds restrains to this goal because the electrons used for imaging interact with matter, requiring samples under high vacuum during imaging. Except for cryo-TEM, this excludes the observation of samples in their natural, hydrated state.

The second, main restrain introduced by electrons is the thickness of the sample: only thin samples can be observed by TEM, whereas most biological samples are soft, which makes the preparation of thin slices impossible.

Therefore, samples have to be prepared adequately for TEM. In general, this involves the arrest of any biological activity by fixation. For morphological studies, conventional TEM preparation at room temperature (RT) relies on aldehyde fixation (Sabatini et al., 1963), followed by a post-fixation with osmium to stabilize lipids (White et al., 1976), and dehydration to replace gradually the water of the sample by an organic solvent. In the final step, the sample is infiltrated with a plastic resin, which becomes hard after polymerization and allows the preparation of thin sections for TEM. In this procedure, each step has well documented artifacts (Kellenberger, 1991), which have to be taken into account. But it should also not be forgotten that these sample preparation protocols have contributed to a vast basis of knowledge before alternative sample preparation methods became available. Characteristic viral factories as seen by TEM of ultrathin sections after conventional embedding are shown in Fig. 3. In mammalian BHK-21 cells,

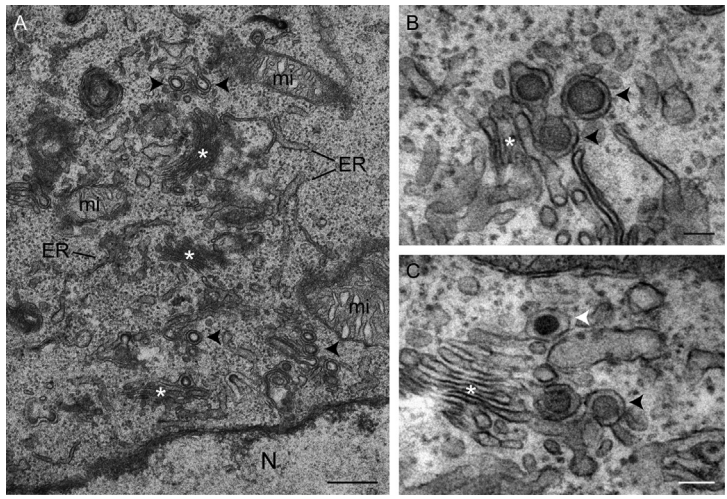


**Fig. 3** Viral factories as seen by TEM of ultrathin sections after conventional embedding. BHK-21 cells were adsorbed with Bunyamwera virus (BUNV) at a MOI of 1 PFU/cell and imaged by TEM at 10 hpi. (A) Low magnification image of a BUNV factory that is a juxtanuclear structure made of Golgi stacks (white asterisks) with spherules (black arrowheads) that contain the VRCs (Fontana et al., 2008), mitochondria (mi) and ER cisternae. N: nucleus. (B and C) High magnification images of BUNV factories showing spherules (black arrowheads) in Golgi stacks (asterisks). A viral particle (white arrowhead) in the lumen of a Golgi sacculus is also seen (white arrowhead in C). Scale bars: 500 nm in A; 100 nm in B and C. Fernández de Castro, unpublished results.

Bunyamwera virus assembles a large cytoplasmic factory using Golgi complex stacks, ER and mitochondria (Fig. 3A). Characteristic spherules with VRCs are formed in Golgi membranes (Fontana et al., 2008) where progeny viruses are assembled (Fig. 3B and C).

## 4. Correlative light and electron microscopy

The term correlative and light electron microscopy (CLEM) covers an enormous area of approaches, different combinations of light microscopy techniques with EM strategies. Two extensive handbooks give an idea about this field, which showed over the last years a very dynamic development and continues to do so (Müller-Reichert and Verkade, 2012, 2014). Therefore, this section does not aim to be exhaustive but should outline examples of different strategies. In general, the different approaches can be defined by the complementing aspects that light microscopy (LM) and EM have in their combination. The light microscope offers an unmatched field of view compared to EM, together with the above discussed possibility of imaging the dynamics of the living sample. On the other side, EM allows to visualize the sample at a higher resolution and in all the structural context of the cell and not only the structures labeled for the light microscope. The different approaches can be grouped: (1) To use the field of view from the light microscope and find a rare event by fluorescent labeling in a population of cells or tissue. After imaging by LM, the sample can be prepared by different methods for EM. (2) Characterize a dynamic process by LM and fix the sample at the event of interest to study it in the context of the cell. (3) Visualize your protein of interest in the context of the cell. Often this approach is done with LM and EM on sections or with cryo-fluorescence followed by cryo-TEM on plunge frozen cells. The latter is reviewed elsewhere (Wolff et al., 2016).

To identify a rare fluorescently labeled event in a culture of infected cells the most straightforward approach is to grow them on a support that has coordinates and can be imaged by LM, allowing to identify the location of the cell. This support can be photoetched glass coverslips or gridded plastic dishes for conventional preparation, sapphire discs with a carbon pattern for high pressure freezing (HPF), or a finder grid for plunge freezing (Madela et al., 2014; Santarella-Mellwig et al., 2018; Tenorio et al., 2018). The pattern on the substrate allows to localize the cell of interest by phase contrast. After embedding in resin the pattern is present on the surface of the resin and will allow to locate the area with the cell of interest and prepare serial sections. A visual example of correlation is shown in Fig. 4. For tissue,

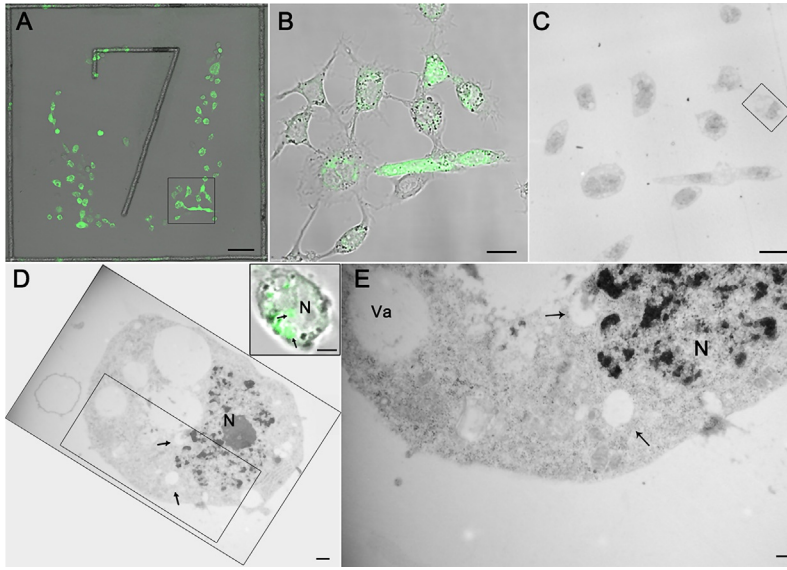


**Fig. 4** Correlative light electron microscopy (CLEM) of viral factories. C6/36 mosquito cells grown on gridded plates were adsorbed with the fluorescent bunyavirus eGFP-Gc-BUNV for 24 h and imaged using phase contrast and fluorescence microscopy at 200× and 630× magnification (A and B, respectively). Gc is one of the glycoproteins of the virus and a marker of viral factories. Ultrathin sections of selected cells (square in A) were imaged by TEM at low magnification (C) and at higher magnification (D and E). (D) TEM image (mainfield) and confocal image (inset) of the cell selected in (C). The arrows point to fluorescent zones (inset) and the approximate corresponding areas in the TEM image. (E) High magnification image shows that the marked fluorescent zones (inset in D) contain vacuole–like structures (arrows). N, nucleus; Va, vacuole. Scale bars: 50 μm in A; 10 μm in B and C; 0.5 μm in D; 5 μm in inset in D; 200 nm in E. Tenorio, unpublished results.

transfer of coordinates provides often a challenge. Fluorescent dyes can be used to highlight specific structures of tissues and create internal landmarks to position the region of interest and embed the samples for EM in such a way that the fluorescence is retained, and either the block or the sections can be imaged by LM (Lucas et al., 2012). Another approach introduced landmarks on the surface of the tissue by an infrared laser (Karreman et al., 2014).

CLEM on sections after sample preparation for EM has the advantage to minimize changes between the LM and EM image, which result from sample preparation. It can be done on Tokuyasu sections (Oorschot et al., 2014), or on methacrylate resins (Kukulski et al., 2011). For both methods, protocols are available that can preserve the fluorescent signal of fluorescent fusion proteins. Alternatively, antibody labeling can be done

on sections (Oorschot et al., 2014; Schwarz and Humbel, 2014). The fluorescent signal can be observed in the LM and afterward the grids are contrasted and observed by EM. Because in the EM the section itself is devoid of landmarks, a first correlation can be obtained with a finder grid. Finer correlation is possible when the DNA inside the nuclei of cells is stained with DAPI or Hoechst for LM. Higher precision can be obtained when fluorescent spheres are applied as landmarks to the section, though this approach requires TEM tomography since the spheres are not visible in a 2D projection image. With this approach it was possible to detect a single HIV-eGFP-delEnv particle at the plasma membrane of a MDCK cell (Kukulski et al., 2011).

Live cell imaging combined with EM allows to study the dynamics of a process and arrest it at the point of interest with the aim of visualization within the context of the cell. The method of live cell imaging depends on the dynamics of the studied process and the resolution required. As mentioned above for imaging live cells, care needs to be taken to avoid phototoxicity. The ideal arrest of the cell after imaging would be cryofixation due to its rapidity. However, this is often limited by practical issues. Often a cryoplunge freezer or a high-pressure freezer are not localized next to a light microscope. And even if they are, the transfer has to be fast enough not to lose the benefit of rapid immobilization. Transfer should also avoid changes in the environment (temperature, physical bending on grid, etc.), which can influence the sample's morphology. Currently there are two ways to combine fast transfer of sapphire discs from the light microscope to a high-pressure freezer (Heiligenstein et al., 2014; Verkade, 2008), both of which allow a short time frame of live cell imaging before high pressure freezing. If biosafety or the length of imaging does not permit this, chemical fixation is mandatory. The delay of the fixation depends on the localization of the process inside the sample. For rat liver, a 4% Paraformaldehyde solution penetrated the tissue to a depth of 2.5 mm within 4 h, which corresponds on average to a penetration of about 170 nm/s (Dempster, 1960). Thus, for events near the plasma membrane like the transport of viral particles for release, chemical fixation will work faster than for the fixation of a viral factory in the centre of the cell. However, it might not be fast enough to visualize fusion or budding events at the plasma membrane. It is still recommendable to control the localization of the event of interest after chemical fixation by light microscopy before processing for EM, either by cryofixation (plunge freezing or high-pressure freezing/HPF), or conventional preparation.

CLEM approaches are advancing our understanding of the biogenesis of viral replication organelles (Bykov et al., 2016). Some interesting examples

include the flaviviruses hepatitis C virus (HCV) and Dengue virus (DENV), the alphavirus Semliki Forest Virus (SFV), the enterovirus coxsackievirus B3, and the human reovirus. The genome replication sites of HCV have been located in a complex vesicular network interconnected with the ER known as the "membranous web" (Paul et al., 2013). This structure originates by accumulation of ER-derived double-membrane vesicles (DMVs). CLEM showed that NS5A, a phosphoprotein that facilitates viral replication by interacting with other viral non-structural proteins and cell factors, accumulates in double-membrane vesicles that locate close to lipid droplets, a key organelle for HCV morphogenesis (Filipe and McLauchlan, 2015; Romero-Brey et al., 2012). These results provided evidence of the spatial connection between HCV genome replication and viral particle morphogenesis inside viral factories. In the case of DENV, CLEM is assisting in the characterization of the biogenesis of the replication factories, in particular in the role of viral proteins in membrane remodeling and virion morphogenesis (Bykov et al., 2016; Scaturro et al., 2015). CLEM allowed the unambiguous identification of the enterovirus coxsackievirus B3 replication organelle morphologies as a first step to understand the requirements for their biogenesis and their evolution over time (Van der Schaar et al., 2016). For the alphavirus SFV, CLEM demonstrated that the spherules with VRC are first formed on the plasma membrane to end up in cytoplasmic vacuoles upon internalization (Spuul et al., 2010). Viral and cell factors required for spherule biogenesis were also studied by CLEM (Kallio et al., 2013; Spuul et al., 2011). A combination of live cell imaging and CLEM unveiled that nascent reovirus replication organelles, known as viral inclusions (VI) are made of aggregates of tubules and vesicles originated by remodeling of the peripheral endoplasmic reticulum and that two reovirus non-structural proteins, σNS and μNS, are responsible for ER remodeling (Tenorio et al., 2018). Besides, CLEM has great potential for evaluating compounds to treat viral infections (Berger et al., 2014; García-Serradilla et al., 2019; Lowen et al., 2018; Martínez et al., 2014). For those interested in performing CLEM of virus-infected cells, detailed, step-by-step CLEM workflows describing sample preparation, imaging and correlation, have been published recently (Hellström et al., 2015; Santarella-Mellwig et al., 2018).

## 5. High-pressure freezing and freeze-substitution

The arrest of cells by chemical fixation is determined by the diffusion of the fixative into the cell and might take seconds. This results in a gradient: first proteins at the plasma membrane are inactivated, whereas intracellular organelles are reached by the fixative at a later time point. To circumvent

this problem, an alternative is to freeze cells fast, which arrests them in their state in milliseconds. However, to keep all cellular structures in place, it is mandatory to vitrify the water in the sample and avoid formation of ice crystals during freezing. At atmospheric pressure this requires high cooling rates and allows only the vitrification up to a thickness of a few micrometers (Escaig, 1982). Bulk samples can be vitrified by high pressure freezing. In this approach, for a few milliseconds a pressure of more than 2000 bars is applied to the sample before cooling is applied (Riehle and Hoechli, 1973). Since water in the liquid state is almost incompressible, the application of the high pressure has no influence on the sample's morphology. But the pressure changes the physical properties of water by lowering the melting point and the temperature for homogenous ice nucleation (Kanno et al., 1975). Depending on the water content of the sample, this allows the vitrification of samples up to 200 μm thickness. After HPF, the sample can be processed and imaged in the frozen state by cryo-FIB (Focused Ion Beam)/cryo-TEM or by CEMOVIS (Cryo-Electron Microscopy of Vitreous Sections) (Hagen et al., 2015; Hayles et al., 2010). Most often the samples are processed by freeze substitution (FS). During FS, the water of the sample is replaced by an organic solvent that contains chemical fixatives to stabilize the sample during warm up. Here, the order of events is the reverse to the above described conventional preparation at RT: during FS the sample is first dehydrated (usually at −90 °C, where chemical fixatives are not active) and then fixed when the temperature is raised (Hurbain and Sachse, 2011). Dehydration in the cold avoids most artifacts of dehydration at RT (Kellenberger, 1991). Since the solvent is also the carrier of the fixatives, these are in place and ready to react with the sample and the gradient of fixation at RT is omitted as well. After dehydration, samples can be infiltrated with a resin that permits immunolabeling, such as Lowicryl- or LR-resins, or in epoxy resin for pure morphological studies.

The advantage of HPF is the fast immobilization of the sample from the native, unfixed state. The fast immobilization permits to catch high dynamic processes that are difficult to visualize by slow chemical fixation, such as cytoskeleton changes, budding or fusion processes (Bilý et al., 2015; Fontana et al., 2010; Wan et al., 2015). However, for virus-infected cells this raises the issue of biosafety. With one exception, most HPF machines are not mobile and it is impossible to move them into a BSL-2 or BSL-3 laboratory. In this case the sample should be inactivated by aldehyde fixation. The advantage of a fast immobilization is lost but a superior morphology can be achieved even with prefixed samples by HPF/FS compared to conventional preparation because the major harm to morphological

preservation is caused by the dehydration step at RT in the latter (Kellenberger, 1991; Sosinsky et al., 2008). However, depending on the virus and the stress the viral infection causes to the host cell, HPF/FS might not be suitable. It has been reported that stressed cells can freeze poorly with ice crystal formation (McDonald, 2007).

For some viruses, HPF/FS allows visualization of viral structures that remain invisible after conventional preparation protocols. This is the case of Foot-and-mouth disease virus (FMDV). The intracellular particles of this virus are not visible by conventional preparation techniques but in cells processed by HPF/FS, newly formed virions are easily seen (Monaghan et al., 2003). This is apparently due to a high sensitivity of viral particles to low pH during conventional sample processing. An example of viral replication organelles visualized by TEM after conventional embedding or HPF/FS is shown in Fig. 5. Viral inclusions (VIs) that are the replication neoorganelles of the human reovirus (Desmet et al., 2014; Rhim et al., 1962), present a more homogeneous content after HPF/FS (compare Fig. 5A and B). Fine structural details such as the morphology of viral particles inside VIs are better preserved after HPF/FS (Fig. 5A and B, insets).

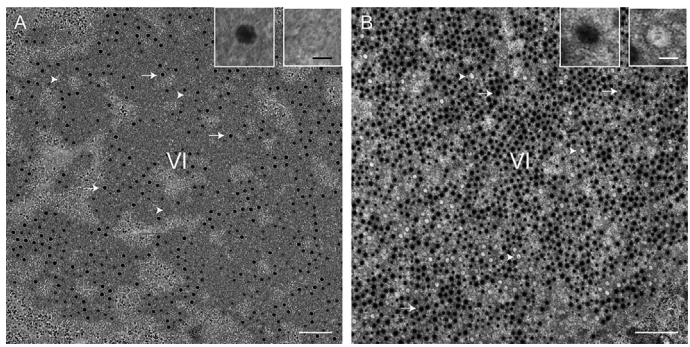


**Fig. 5** Conventional embedding vs HPF/FS of human reovirus inclusions. Human brain microvascular endothelial cells (HBMECs) were infected with reovirus at a MOI of 1 PFU/cell. At 18 hpi, cells were fixed with aldehydes and either dehydrated with ethanol at 4 °C and embedded in EML-812 epoxy resin (A) or processed by high-pressure freezing, freeze-substitution and embedding in EML-812 (B). Ultrathin sections show that the reovirus replication organelles known as viral inclusions (VIs) have empty areas after conventional embedding (A) but a more homogeneous content after HPF/FS (B). Both mature virions (arrows) and empty viral particles (arrowheads) are easily distinguished in VIs after either conventional preparation or HPF/FS. Higher magnification views of individual viral particles (insets) show that fine details in both mature virions and empty viral particles are better appreciated after HPF/FS. Scale bars: 500 nm in main fields, 50 nm in insets. Fernández de Castro, unpublished results.

Another viral RO studied by HPF/FS is that assembled by Rubella virus (RUBV) in modified lysosomes that are surrounded by RER cisternae and mitochondria (Fontana et al., 2007; Lee et al., 1994; Magliano et al., 1998). HPF/FS has shown fine details of the complex organization of these structures such as arrays of filaments surrounding the ROs, macromolecular complexes connecting the RO with RER and mitochondria, spherules connected with flat membranes that contain macromolecules organized in oligomeric arrays inside the RO, and pores opened to the cytosol on the periphery of the RO (Fontana et al., 2010). Furthermore, HPF/FS is helping to understand how remodeled membranes build very large viruses such as vaccinia virus and the giant Mimivirus (Milrot et al., 2016; Mutsafi et al., 2013; Suárez et al., 2013).

## 6. Frozen-hydrated sections: Cemovis and cryo-lamella

HPF increases the depth of vitrification in the sample but in a TEM only thin specimens can be visualized. After the discovery of vitrified water and the onset of cryo-EM (Brüggeller and Mayer, 1980; Dubochet and McDowall, 1981) the transition from thin films of vitrified small biological specimens to vitrified sections of bulk specimen was fast (Lepault et al., 1983; McDowall et al., 1983). To prepare a sample for cryo-electron microscopy of vitreous sections (CEMOVIS), first the sample and the surrounding medium is vitrified. Next, it is sectioned in a cryo-microtome below the devitrification temperature of pure water and the sections are transferred to a grid. The sections are observed in the frozen state with a cryo-TEM using low dose conditions. For a long time, CEMOVIS was the only approach for cryo-TEM of bulk specimens. Compared to the thin film method of plunge frozen material, a frozen hydrated section has artifacts, mainly knife marks, compression, and crevasses of which the last two can be controlled (Al-Amoudi et al., 2005). CEMOVIS offers to visualize at high resolution a section of a bulk sample close to the native state. As for all cryo-EM approaches, also for CEMOVIS it is important to minimize the radiation damage of the beam during imaging. Though beam damage takes place also for resin embedded samples and results in shrinkage and mass loss (Luther et al., 1988). Nevertheless, this is mainly a concern for tomography of resin embedded material because the implications for 2D projection images of thin sections are negligible. By contrast, in cryo-EM of hydrated specimens beam damage is also visible on 2D projection images, which is impressively seen by the phenomenon of bubbling of organic

material after a certain amount of electron dose (Dubochet et al., 1982). Bubbling is caused by $H_2$ formation due to radiolysis of the biological specimen and the onset of it depends on the composition of the sample. On CEMOVIS sections it often starts on membranes or in protein rich regions. However, the structural damage starts already at low doses of electrons (Lepault et al., 1983). In our hands a dose between 5 and 8 e/Å$^2$ per image allows at 120 kV to take images at several defocus values. For TEM tomography of CEMOVIS sections the cumulative dose should be kept below 80 e/Å$^2$ (Hagen and Grünewald, 2008). However, for TEM tomography the use of CEMOVIS sections has remained a challenge, which is mainly due to the difficulties to attach the whole section flat on the grid and the pronounced formation of crevasses on sections thicker than 60 nm but it is not impossible (Bouchet-Marquis and Hoenger, 2011; Hagen et al., 2015). To avoid these problems for TEM tomography of vitreous sections, the preparation of cryo-lamella by FIB-SEM (Scanning Electron Microscopy) has been developed during the last years (Hagen et al., 2015; Hayles et al., 2010). Infected cells are plunge frozen on a TEM grid and are thinned in the FIB. With the absence of compression and especially crevasses, the sample is better suited for TEM tomography than a CEMOVIS section. However, care needs to be taken to thin the area of interest since a big part of the cell is removed by the FIB (Arnold et al., 2016). A current drawback of this approach is the cost of the equipment.

Not used yet to study viral replication organelles and VRCs, CEMOVIS has shown the structures associated to assembly and movement of large viruses within cells (Hagen and Grünewald, 2008; Suárez et al., 2013) and has a great potential to visualize the native organization of viral and cellular macromolecular complexes that build and work inside viral factories.

## 7. Immunogold labelling

For all immunolabeling approaches a high affinity probe binds specifically to its target. The probe is either directly linked to an electron dense marker that can be directly visualized in the TEM or detected indirectly with a secondary probe, which carries an electron dense marker. Ferritin was used in the past to be later substituted by colloidal gold probes (Singer and Schick, 1961; Slot and Geuze, 1981). The majority of high affinity probes used today are antibodies against proteins, but also lectins can be used and in situ hybridization for RNA localization is possible (Gershon et al., 1994; Herpers et al., 2010). Different strategies exist to label the target of interest: they can be

divided in general between pre- and post-embedding labeling. For pre-embedding labeling the whole cell is incubated with the affinity probe, followed by the electron dense marker. However, without permeabilization only epitopes exposed to the exterior of the cell are accessible (Gelderblom et al., 1987; Hinners et al., 1999). Permeabilization will provide access to intracellular epitopes, but will extract also cellular material and result in a compromised morphology. For post-embedding labeling, the sample is embedded in a way that preserves the structure of the epitope so that the affinity probe can bind to it when exposed on the surface of the section. This can be done when the samples are embedded in an acrylic or methacrylic resin, as LR White or Lowicryl (Armbruster et al., 1982; Ellinger and Pavelka, 1985). Methacrylic resins were developed by the group of Villiger-Kellenberger. They do not chemically react with the sample, and exist with a versatile range of polarities, which makes them compatible with immuno labeling (Carlemalm et al., 1982). An alternative for resin embedding is labeling on thawed cryosections, an approach which is also called the Tokuyasu technique, after its pioneer Kiyoteru Tokuyasu (Möbius and Posthuma, 2019). In this approach, the sample is arrested by a mild chemical fixation with aldehydes. Since chemical fixation is mandatory, in this approach it can be combined with the often necessary inactivation of viruses presenting a biosafety risk. Chemical fixation makes the plasma membrane of cells permeable for small solutes and the sample can be infiltrated with a sucrose solution (Penttila et al., 1974; Tokuyasu, 1973). The sucrose has a dual role: first, it works as a cryo-protectant for the subsequent freezing step, and second, it influences the elasticity of the sample to facilitate cryo-sectioning. After cryo-protection, the sample can be frozen in liquid nitrogen and becomes hard enough to be sectioned in a cryo-microtome. Frozen sections are thawed and transferred to a grid. Once attached to a grid they can be immunolabeled. The mild fixation of the sample combined with the absence of dehydration results in a good preservation of antigenicity for proteins. Together with the secondary probes conjugated to colloidal gold with different, defined size, this technique allows to study the distribution of two up to three different proteins in one labeling experiment (Slot and Geuze, 1981). But it is important to have the right controls for the specificity of the labeling (Möbius and Posthuma, 2019). After the labeling, the sections are embedded in a thin film of a mixture of uranylacetate and methylcellulose (Griffith et al., 1982). The uranylacetate works as a contrast agent, whereas the methylcellulose provides support to avoid too much shrinkage during the air-drying of the—until this moment—hydrated sections. With uranylacetate as

the only contrasting agent the image of the sample from a Tokuyasu section gives a mixture of positive (e.g., nucleus) and negative contrast (e.g., membranes) with certain cellular structures (microtubules, ribosomes) unstained. The selective staining is more than compensated by the good preservation of antigens. The possibility of double or triple labeling makes it possible to study the distribution and sorting of viral proteins during their synthesis, and identify their pathways by cellular markers. This was elegantly demonstrated in the studies of the morphogenesis of the human immunodeficiency virus (HIV) in macrophages (Deneka et al., 2007). With the help of immunogold labeling on Tokuyasu cryosections, the authors demonstrated that the virus assembles in an intracellular membranous compartment that contains several tetraspanins and that is connected with the plasma membrane. Immunogold labeling contributed also to identify the cytoplasmic replication organelles of Vaccinia Virus (VV) that are endoplasmic reticulum-enclosed mini-nuclei (Tolonen et al., 2001) and to visualize the connections of nascent VV particles with ER/ERGIC cellular membranes that participate in the assembly of immature viruses (Moss, 2015; Salmons et al., 1997). Localization of viral proteins and cell markers helps to explore the origin of viral replication organelles. Moreover, assays of brome-uridine or brome-deoxiuridine incorporation for RNA or DNA viruses, respectively, in combination with immunogold detection on Tokuyasu cryosections, have been very useful to identify active replication organelles (Besse and Puvion-Dutilleul, 1994; Fontana et al., 2008; Tenorio et al., 2018). An example is shown in Fig. 6. Reovirus VIs are labeled with antibodies specific for ER markers, such as the protein disulfide isomerase (PDI) (Fig. 6A). These organelles support viral genome replication because in the presence of inhibitors of cellular RNA synthesis, they incorporate BrU, as confirmed with specific antibodies in immunogold labeling assays (Fig. 6B). For RNA viruses, antibodies specific for double-stranded RNA, an intermediate formed during RNA replication, are also used to label active VRCs. Anti-dsRNA antibodies work particularly well for positive-sense RNA viruses (Cotton et al., 2017; Fontana et al., 2007; Welsch et al., 2009) and some negative-sense RNA viruses (Fontana et al., 2008; Mateer et al., 2019). For bunyaviruses and flaviviruses it has been demonstrated that the anti-dsRNA signal co-localizes with that of BrU incorporation sites (Fontana et al., 2008; Westaway et al., 1999).

An important advantage of immunogold labeling is that quantitative analysis of the distribution or the labeling densities of the protein of interest is easy to perform (Mayhew, 2005).

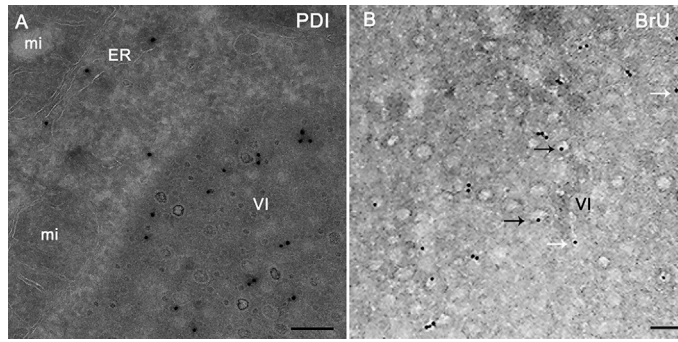


**Fig. 6** Immunogold labeling in Tokuyasu cryosections of reovirus inclusions. HeLa cells were adsorbed with reovirus and incubated for 24 h (A) or 14 h (B), fixed with aldehydes, cryoprotected, frozen in liquid nitrogen, and sectioned at −120 °C. (A) Thawed cryosections were processed for immunogold labeling using an anti-PDI antiserum and a secondary antibody bound to 10-nm colloidal gold particles. Anti-PDI antibody labels RER cisternae in the cytosol and membranes inside inclusions. (B) Cells were processed to localize viral RNA synthesis with a bromouridine (BrU) incorporation assay. The thawed cryosection was labeled with an anti-BrU antibody and a secondary antibody bound to 10-nm colloidal gold particles. Inside the VI, the anti-BrU antibody labels viral particles (black arrows) and membrane fragments (white arrows) VI, viral inclusion; RER, rough endoplasmic reticulum; mi, mitochondrion. Scale bars: 200 nm in A; 100 nm in B. *Modified from Tenorio, R., Fernández de Castro, I., Knowlton, J.J., Zamora, P.F., Lee, C.H., Mainou, B.A., Dermody, T.S., Risco, C. 2018. Reovirus σNS and μNS proteins remodel the endoplasmic reticulum to build replication neo-organelles. mBio 9, e01253-18.*

## 8. 3D imaging/tomography

The images that a transmission electron microscope generates from a thin section are 2D projections of the 3D volume of the section. In this projection, the spatial information within the volume of the thin section is lost. Over the last decades different 3D imaging techniques for biological samples have evolved. In general, for the different approaches there is an inverse relation between the resolution that can be obtained and the volume that can be imaged. TEM electron tomography (TEM-ET) started with the groundbreaking work of Hoppe et al. (1974). For ET, a series of 2D projection images of a sample is acquired over a large tilt series (+70° to −70°) in small increments of 1° (Frank, 1995) and the 3D model of the sample is computationally reconstructed. Due to the geometry of the sample holder, images at tilts above 70° are impossible to acquire and a part of the sample will be lost in the reconstruction (missing wedge). For plastic sections, this wedge can be reduced and the resolution of the final tomogram increased by the

acquisition of a double tilt series (Mastronarde, 1997). TEM-ET offers a good resolution but is limited by the thickness of the section that can be visualized (maximum 300–500 nm), and the size of the area that can be analyzed. STEM (Scanning Transmission Electron Microscopy) tomography allows the acquisition of tilt series from thicker sections up to 700 nm (Yakushevska et al., 2007).

FIB-SEM tomography allows the study of larger volumes than TEM tomography (De Winter et al., 2009). The sample is inside an SEM, which is equipped with a second, ion beam column. The blockface of a resin embedded sample is imaged by the backscattered electrons or the secondary electrons of the beam. After imaging the ion beam removes a layer of 5–10 nm of the sample and prepares a new blockface for imaging. Compared to TEM tomography, the resolution is lower but volumes up to $20 \times 20 \times 20\,\mu m^3$ can be analyzed (Titze and Genoud, 2016).

For serial sectioning tomography, serial sections are collected on slot grids and the 3D volume of the sample is combined by the stacking of the 2D projections data from each single section (Harris et al., 2006). Therefore, the resolution in X and Y is down to few nanometers while in Z it is determined by the section thickness. Compared to FIB-SEM, serial sections are a non-destructive approach because the sections can be stored and re-evaluated. It also allows the reconstruction of large volumes and even whole cells can be studied. To avoid the difficulties of serial section tomography that come with varying compression and folds, Denk and Horstmann (2004) placed the sample into an SEM that contains a microtome. The image of the blockface is generated by the backscattered electrons of the SEM beam and after imaging, the microtome removes 30–50 nm of the sample surface to prepare a new blockface. Due to the imaging in the SEM, the resolution is lower compared to TEM serial section tomography, but larger volumes can be analyzed.

Three-dimensional imaging of viral infections is showing how much viruses modify the cell architecture to build their own structures for viral genome replication, morphogenesis, egress and propagation (Bilý et al., 2015; Chlanda et al., 2009; Earl et al., 2013; Felts et al., 2010; Gómez-Aix et al., 2015; Ibiricu et al., 2011; Milrot et al., 2016; Mutsafi et al., 2010, 2013, 2014; Villinger et al., 2015; Wan et al., 2015; Welsch et al., 2009). The first study of a viral replication organelle visualized in 3D by electron tomography showed that flock house virus (FHV) in Drosophila cells assembles spherules with VRCs in mitochondria, spherules that connect with the cytosol through pores (Kopek et al., 2007). The 3D characterization of SARS CoV and DENV replication platforms

had a significant impact in the field (Knoops et al., 2008; Welsch et al., 2009). Since then, many studies have demonstrated the power of these methods. Structures harboring the VRCs such as single-membrane spherules and double membrane vesicles have been studied in detail within the replication organelles of West Nile Virus (Gillespie et al., 2010), HCV (Romero-Brey et al., 2012), coxsackievirus B3 (Limpens et al., 2011), Bunyamwera virus (Fontana et al., 2008), Rubella virus (Fontana et al., 2010), Tombusvirus (Fernández de Castro et al., 2017a), a cardiovirus (Melia et al., 2018) and the human reovirus (Fernández de Castro et al., 2014a; Tenorio et al., 2018). The reovirus replication neoorganelle visualized in 3D with two different methods is shown in Fig. 7. With 3D reconstruction of serial sections large volumes that contain whole viral factories were

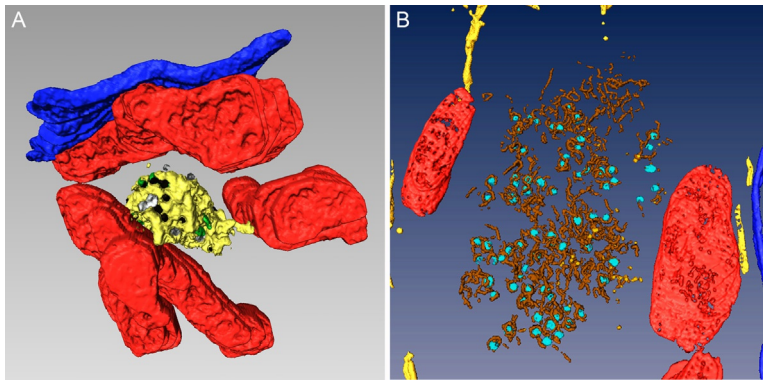


**Fig. 7** 3D models of reovirus inclusions. (A) HeLa cells were adsorbed with reovirus and fixed at 12 hpi. The inclusion was visualized by TEM of serial sections, 3D volume reconstruction, and image processing. The VI contains a network of membranes (yellow) surrounded by mitochondria (red). The inclusion is adjacent to the nuclear envelope (blue). Inside the VI, mature virions (black), empty viral particles (white) and microtubules (green) are integrated in the membranous network. (B) Reovirus-infected cells were fixed at 14 hpi, frozen in liquid nitrogen, and sectioned at −120 °C following the Tokuyasu method. Thawed cryosections were processed by electron tomography. RER cisternae (yellow), mitochondria (red), nuclear envelope (dark blue) are close to the viral inclusion. The VI is a collection of tubules (brown) and vesicles (orange) with viral particles (light blue) attached to membranes. Although reoviruses are non-enveloped particles, we hypothesize that VI membranes might provide physical support for viral genome replication or particle assembly. *Panel (A): Reproduced from Fernández de Castro, I., Zamora, P.F., Ooms, L., Fernández, J.J., Lai, C.M., Mainou, B.A., Dermody, T.S., Risco, C., 2014a. Reovirus forms neo-organelles for progeny particle assembly within reorganized cell membranes. mBio 5, e00931-13 and Panel (B): Tenorio, R., Fernández de Castro, I., Knowlton, J.J., Zamora, P.F., Lee, C.H., Mainou, B.A., Dermody, T.S., Risco, C. 2018. Reovirus σNS and μNS proteins remodel the endoplasmic reticulum to build replication neo-organelles. mBio 9, e01253-18.*

generated (Fig. 7A). With ET of Tokuyasu cryosections smaller volumes with better definition of membranes and higher resolution were obtained (Fig. 7B).

3D imaging has revealed that inside viral factories there are inter-organelle contacts not observed in non-infected cells (Fontana et al., 2010; Risco et al., 2014). Some reports show that structures with VRCs localize close to virus assembly sites, something expected but difficult to detect in two dimensions (Fontana et al., 2008; Welsch et al., 2009). One of the current technical challenges is the development of labeling methods for localizing viral and cellular macromolecules in three dimensions.

## 9. Clonable tags for electron microscopy

Electron microscopists have been working for decades to localize proteins in cells in two and three dimensions. Together with the fundamental contribution of antibodies and immunogold labeling assays described in Section 7, a number of approaches have been reported to label proteins in cells using clonable tags. Most of them are based on the generation of an electron-dense precipitate of diaminobenzidine as a result of photoactivation of a fluorophore (GFP or Mini-SOG) or an enzymatic reaction (HRP or APEX2) (Connolly et al., 1994; Grabenbauer et al., 2005; Martell et al., 2012). An alternative approach that uses the small metal binding protein metallothionein (MT) as a clonable tag for electron microscopy was proposed by two scientists working at Brandeis University (Mercogliano and DeRosier, 2006, 2007). The idea of MT-tagging was the basis of METTEM (Metal-Tagging TEM), a highly sensitive labeling technique that was validated in bacteria (Diestra et al., 2009a, 2009b), yeast (Barajas et al., 2014; Morphew et al., 2015), and mammalian cells (Fernández de Castro et al., 2017b; Risco et al., 2012; Sachse et al., 2018; Tenorio et al., 2018) and the only one used so far to label intracellular viral structures. In live cells incubated briefly with gold salts, proteins bearing MT will form ~1 nm-gold nano-clusters, readily detectable by electron microscopy (Risco et al., 2012). If the protein of interest is fused with MT and a fluorescent tag such as GFP, the same molecules will be visualized by light and electron microscopy (Fernández de Castro et al., 2014b). Combining METTEM with immunogold allows double and multiple labeling approaches (Fernández de Castro et al., 2014b). MT-tagging was used to detect one of the proteins of the Rubella virus VRC within replication organelles (ROs) (Risco et al., 2012). The study revealed that the viral polymerase molecules first localized in the plasma membrane to be later transported to lysosomes/ROs, where they aggregate into

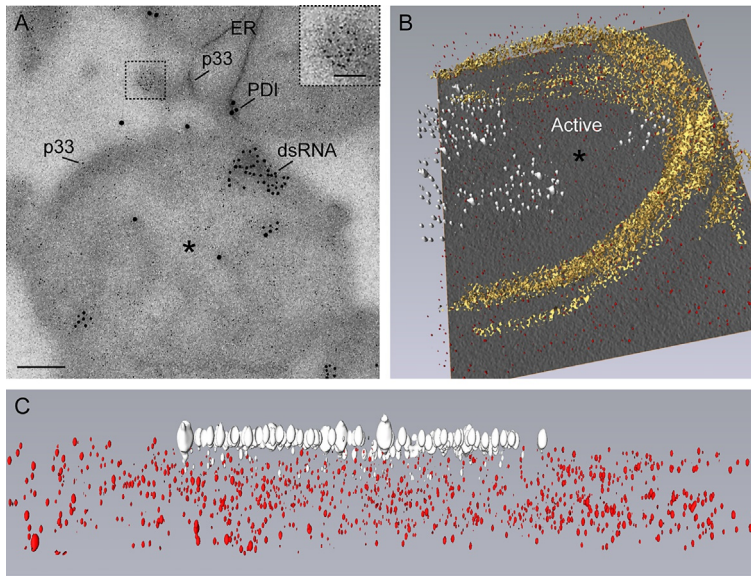


**Fig. 8** METTEM of viral replication organelles. *Saccharomyces cerevisiae* Δpah1 cells expressing p33, the most abundant VRC component of the plant virus TBSV (Tomato Bushy Stunt Virus), fused with MT tag as a viral replicon component were incubated with gold salts, embedded in the resin LR White, sectioned, immunogold labeled and visualized by 2D TEM (A) or electron tomography (B and C). (A) METTEM visualization of p33-MT-gold nanoparticles (~1 nm) in an unstained ultrathin section. p33-MT-gold was detected inside the replication organelle (black asterisk) and in the surrounding ER membranes, that were labeled with an anti-PDI antibody and a secondary antibody conjugated with 10 nm colloidal gold particles. Replicating TBSV RNA was labeled with an antibody against dsRNA and a secondary antibody conjugated to 5-nm gold particles. The inset is a high magnification of a group of p33-MT-gold nanoclusters. (B) Electron tomography of active VRCs within the replication organelle. Before ET, sections were processed by immunogold labeling with an antibody against dsRNA and a colloidal gold conjugate (white). Molecules of p33-metallothionein-gold are represented in red and ER membranes in yellow. The active domain labeled with antibodies (black asterisk) within the replication organelle is surrounded by ER membranes, whereas the domain beyond the ER boundaries is not labeled. (C) Lateral view of the tomogram in B, showing the anti-dsRNA antibodies bound to their antigens on the section surface (white), whereas p33 molecules (red) were detected inside the section. Scale bar: 100 nm in mainfield in A; 50 nm in inset in A. *Modified from Fernández de Castro, I., Fernández, J.J., Barajas, D., Nagy, P.D., Risco, C., 2017a. Three-dimensional imaging of the intracelular assembly of a functional viral RNA replicase complex. J. Cell Sci. 130, 260–268, with permission.*

densely packed oligomeric arrays. Studies with the Tombusvirus Tomato Bushy Stunt Virus (TBSV) showed the distribution of the viral replicase molecules in modified ER membranes within the replication factory (Barajas et al., 2014) (Fig. 8). Molecules of the p33-MT-gold subunit of the viral polymerase

labeled in live cells were visualized as ~1 nm nano-clusters in ultrathin sections (Fig. 8A). Immunogold labeling on sections confirmed the association of p33-MT-gold molecules with ER membranes labeled with anti-PDI antibodies and with active replication sites labeled with anti-dsRNA antibodies (Fig. 8A). 3D maps of the replicase molecules inside replication organelles were obtained by electron tomography (Fernández de Castro et al., 2017a) (Fig. 8B). These volumes showed RO active domains labeled with anti-dsRNA antibodies together with RO domains devoid of labeling. A lateral view of the tomogram is shown in Fig. 8C. This volume shows why METTEM is a labeling method of high sensitivity: with antibodies only the epitopes exposed on the surface of the section are detected; however, with METTEM all protein molecules carrying an MT-gold-nanocluster inside the section are visualized in 2D and 3D. With METTEM it was discovered that influenza virus uses a modified ER to transport the vRNPs from the nucleus to the plasma membrane in a process that depends on Rab11 (Fernández de Castro et al., 2017b). Early in infection, the reovirus non-structural protein μNS fused with MT was found in strangled ER cisternae and small vesicles near the nucleus. This result suggests that μNS triggers the massive ER fragmentation that generates replication organelles by direct binding to ER membranes (Tenorio et al., 2018).

New developments and improvements for METTEM are in progress. Combining METTEM with CEMOVIS will allow ultrastructural imaging of viral macromolecular complexes in intracellular viral factories in their native state and at molecular scale resolution.

## 10. Conclusions and future perspectives

Recent advances in sample preparation and imaging by light and electron microscopy are having considerable impact in virology. The powerful combination of different imaging techniques with various levels of resolution shows the viral life cycle from the early steps of virus entry and replication to the final stages of viral particle morphogenesis and egress. All these processes take place at different locations in the infected cell, and after the initial study of infection in live cells, scientists can focus on the subsequent characterization of particular structures at high resolution by electron microscopy. All techniques have advantages and limitations, as summarized in Fig. 1, and the choice of methods depends on the complexity of the study.

Some technical challenges for the future include developing super-resolution light microscopy for live cells, improve CLEM protocols, new image processing tools for 3D TEM, and combining molecular mapping methods such as METTEM with Tokuyasu cryosections and CEMOVIS. The myriad of structural data to be obtained will help to interfere with the biogenesis and function of viral structures in cells. Drugs that block the construction of functional replication organelles, assembly sites and virus egress machineries will be the basis of new antiviral strategies.

## Acknowledgments

The authors acknowledge Prof. Terence S. Dermody and his team at the University of Pittsburgh for many useful discussions and Dr. Laura Sanz-Sánchez for data in Movie 1 in the online version at https://doi.org/10.1016/bs.aivir.2019.07.005 and Fig. 2. This work has been supported by grant BIO2015-68758-R (AEI/FEDER, EU) from the Ministry of Science, Innovation and Universities of Spain.

## References

Abernathy, E., Mateo, R., Majzoub, K., van Buuren, N., Bird, S.W., Carette, J.E., Kirkegaard, K., 2019. Differential and convergent utilization of autophagy components by positive-strand RNA viruses. PLoS Biol. 17 (1), e2006926.

Al-Amoudi, A., Studer, D., Dubochet, J., 2005. Cutting artefacts and cutting process in vitreous sections for cryo-electron microscopy. J. Struct. Biol. 150, 109–121.

Alonas, E., Vanover, D., Blanchard, E., Zurla, C., Santangelo, P.J., 2016. Imaging viral RNA using multiply labeled tetravalent RNA imaging probes in live cells. Methods 98, 91–98.

Altan-Bonnet, N., 2017. Lipid tales of viral replication and transmission. Trends Cell Biol. 27, 201–213.

Armbruster, B.L., Carlemalm, E., Chiovetti, R., Garavito, R.M., Hobot, J.A., Kellenberger, E., Villiger, W., 1982. Specimen preparation for electron microscopy using low temperature embedding resins. J. Microsc. 126, 77–85.

Arnold, J., Mahamid, J., Lucic, V., de Marco, A., Fernandez, J.J., Laugks, T., Mayer, T., Hyman, A.A., Baumeister, W., Plitzko, J.M., 2016. Site-specific cryo-focused Ion beam sample preparation guided by 3D correlative microscopy. Biophys. J. 110, 860–869.

Baktash, Y., Randall, G., 2019. Live cell imaging of hepatitis C virus trafficking in hepatocytes. Methods Mol. Biol. 1911, 263–274.

Baktash, Y., Madhav, A., Coller, K.E., Randall, G., 2018. Single particle imaging of polarized hepatoma organoids upon hepatitis C virus infection reveals an ordered and sequential entry process. Cell Host Microbe 23, 382–394.

Barajas, D., Fernández de Castro, I., Pogany, J., Risco, C., Nagy, P.D., 2014. Noncanonical role for the host Vps4 AAA + ATPase ESCRT protein in the formation of Tomato bushy stunt virus replicase. PLoS Pathog. 10, e1004087.

Berger, C., Romero-Brey, I., Radujkovic, D., Terreux, R., Zayas, M., Paul, D., Harak, C., Hoppe, S., Gao, M., Penin, F., Lohmann, V., Bartenschlager, R., 2014. Daclatasvir-like inhibitors of NS5A block early biogenesis of hepatitis C virus-induced membranous replication factories, independent of RNA replication. Gastroenterology 147 (1094–1105) e1025.

Besse, S., Puvion-Dutilleul, F., 1994. High resolution localization of replicating viral genome in adenovirus-infected HeLa cells. Eur. J. Cell Biol. 63, 269–279.

Bilý, T., Palus, M., Eyer, L., Elsterová, J., Vancová, M., Růžek, D., 2015. Electron tomography analysis of tick-borne encephalitis virus infection in human neurons. Sci. Rep. 5, 10745.

Bouchet-Marquis, C., Hoenger, A., 2011. Cryo-electron tomography on vitrified sections: a critical analysis of benefits and limitations for structural cell biology. Micron 42, 152–162.

Brüggeller, P., Mayer, E., 1980. Complete vitrification in pure liquid water and dilute aqueous solutions. Nature 288, 569–571.

Bykov, Y.S., Cortese, M., Briggs, J.A.G., Bartenschlager, R., 2016. Correlative light and electron microscopy methods for the study of virus-cell interactions. FEBS Lett. 590, 1877–1895.

Campbell, E.M., Hope, T.J., 2008. Live cell imaging of the HIV-1 life cycle. Trends Microbiol. 16, 580–587.

Carlemalm, E., Garavito, R.M., Villiger, W., 1982. Resin development for electron microscopy and an analysis of embedding at low temperature. J. Microsc. 126, 123–143.

Chlanda, P., Carbajal, M.A., Cyrklaff, M., Griffiths, G., Krijnse-Locker, J., 2009. Membrane rupture generates single open sheets during vaccinia virus assembly. Cell Host Microbe 6, 81–90.

Connolly, C.N., Futter, C.E., Gibson, A., Hopkins, C.R., Cutler, D.F., 1994. Transport into and out of the Golgi complex studied by transfecting cells with cDNAs encoding horseradish peroxidase. J. Cell Biol. 127, 641–652.

Cotton, B.T., Hyde, J.L., Sarvestani, S.T., Sosnovtsev, S.V., Gree, K.Y., White, P.A., Mackenzie, J.M., 2017. The norovirus NS3 protein is a dynamic lipid- and microtubule-associates protein involved in viral RNA replication. J. Virol. 91, e02138-16.

De Winter, D.A., Schneijdenberg, C.T., Lebbink, M.N., Lich, B., Verkleij, A.J., Drury, M.R., Humbel, B.M., 2009. Tomography of insulating biological and geological materials using focused ion beam (FIB) sectioning and low-kV BSE imaging. J. Microsc. 233, 372–383.

Dempster, W.T., 1960. Rates of penetration of fixing fluids. Am. J. Anat. 107, 59–72.

Deneka, M., Pelchen-Matthews, A., Byland, R., Ruiz-Mateos, E., Marsh, M., 2007. In macrophages, HIV-1 assembles into an intracellular plasma membrane domain containing the tetraspanins CD81, CD9, and CD53. J. Cell Biol. 177, 329–341.

Denk, W., Horstmann, H., 2004. Serial block-face scanning electron microscopy to reconstruct three-dimensional tissue nanostructure. PLoS Biol. 2, e329.

Desmet, E.A., Anguish, L.J., Parker, J.S.L., 2014. Virus-mediated compartimentalization of the host translational machinery. mBio 5, e01463-14.

Diestra, E., Fontana, J., Guichard, P., Marco, S., Risco, C., 2009a. Visualization of proteins in intact cells with a clonable tag for electron microscopy. J. Struct. Biol. 165, 157–168.

Diestra, E., Cayrol, B., Arluison, V., Risco, C., 2009b. Cellular electron microscopy imaging reveals the localization of the Hfq protein close to the bacterial membrane. PLoS One 4, e8301.

Dirk, B.S., Van Nynatten, L.R., Dikeakos, J.D., 2016. Where in the cell are you? Probing HIV-host interactions through advanced imaging techniques. Viruses 8, 200. https://doi.org/10.3390/v8100288.

Dubochet, J., McDowall, A.W., 1981. Vitrification of pure water for electron microscopy. J. Microsc. 124, RP3–RP4.

Dubochet, J., Lepault, J., Fremman, R., Berriman, J.A., Homo, J.C., 1982. Electron microscopy of frozen water and aqueous solutions. J. Microsc. 128, 219–237.

Earl, L.A., Lifson, J.D., Subramaniam, S., 2013. Catching HIV "in the act" with 3D electron microscopy. Trends Microbiol. 21, 397–404.

Eichwald, C., Arnoldi, F., Laimbacher, A.S., Schraner, E.M., Fraefel, C., Wild, P., Burrone, O.R., Ackermann, M., 2012. Rotavirus viroplasm fusion and perinuclear localization are dynamic processes requiring stabilized microtubules. PLoS One 7 (10), e47947.

Ellinger, A., Pavelka, M., 1985. Post-embedding localization of glycoconjugates by means of lectins on thin sections of tissues embedded in LR white. Histochem. J. 17, 1321–1336.
Erickson, K.D., Bouchet-Marquis, C., Heiser, K., Szomolanyi-Tsuda, E., Mishra, R., Lamothe, B., Hoenger, A., Garcea, R.L., 2012. Virion assembly factories in the nucleus of polyomavirus-infected cells. PLoS Pathog. 8 (4), e1002630.
Escaig, J., 1982. New instruments which facilitate rapid freezing at 83 K and 6 K. J. Microsc. 126, 221–229.
Eyre, N.S., Fiches, G.N., Aloia, A.L., Helbig, K.J., McCartney, E.M., McErlean, C.S.P., Li, K., Aggarwal, A., Turvilee, D.G., Beard, M.R., 2014. Dynamic imaging of the hepatitis C virus NS5A protein during productive infection. J. Virol. 88, 3636–3652.
Felts, R.L., Narayan, K., Estes, J.D., Shi, D., Trubey, C.M., Fu, J., Hartnell, L.M., Ruthel, G.T., Schneider, D.K., Nagashima, K., Bess Jr., J.W., Bavari, S., Lowekamp, B.C., Bliss, D., Lifson, J.D., Subramaniam, S., 2010. 3D visualization of HIV transfer at the virological synapse between dendritic cells and T cells. Proc. Natl. Acad. Sci. U. S. A. 107, 13336–13341.
Fernández de Castro, I., Volonté, L., Risco, C., 2013. Virus factories: biogenesis and structural design. Cell. Microbiol. 15, 24–34.
Fernández de Castro, I., Zamora, P.F., Ooms, L., Fernández, J.J., Lai, C.M., Mainou, B.A., Dermody, T.S., Risco, C., 2014a. Reovirus forms neo-organelles for progeny particle assembly within reorganized cell membranes. mBio 5, e00931-13.
Fernández de Castro, I., Sanz-Sánchez, L., Risco, C., 2014b. Metallothioneins for correlative light and electron microscopy. Methods Cell Biol., 124, Elsevier, pp. 55–70.
Fernández de Castro, I., Tenorio, R., Risco, C., 2016. Virus assembly factories in a lipid world. Curr. Opin. Virol. 18, 20–26.
Fernández de Castro, I., Fernández, J.J., Barajas, D., Nagy, P.D., Risco, C., 2017a. Three-dimensional imaging of the intracelular assembly of a functional viral RNA replicase complex. J. Cell Sci. 130, 260–268.
Fernández de Castro, I., Fournier, G., Sachse, M., Pizarro-Cerdá, J., Risco, C., Naffakh, N., 2017b. Influenza virus genome reaches the plasma membrane via a modified endoplasmic reticulum and Rab11-dependent vesicles. Nat. Commun. 8 (1), 1396.
Fernández-Oliva, A., Ortega-Gónzalez, P., Risco, C., 2019. Targeting host lipid flows: exploring new antiviral and antibiotic strategies. Cell. Microbiol. 21 (3), e12996.
Filipe, A., McLauchlan, J., 2015. Hepatitis C virus and lipid droplets: finding a niche. Trends Mol. Med. 21, 34–42.
Fontana, J., Tzeng, W.-P., Calderita, G., Fraile-Ramos, A., Frey, T.K., Risco, C., 2007. Novel replication complex architecture in rubella replicon-transfected cells. Cell. Microbiol. 9, 875–890.
Fontana, J., López-Montero, N., Elliott, R.M., Fernández, J.J., Risco, C., 2008. The unique architecture of Bunyamwera virus factories around the Golgi complex. Cell. Microbiol. 10, 2012–2028.
Fontana, J., López-Iglesias, C., Tzeng, W.-P., Frey, T.K., Fernández, J.J., Risco, C., 2010. Three-dimensional structure of Rubella virus factories. Virology 405, 579–591.
Francis, A.C., Melikyan, G.B., 2018. Live-cell imaging of early steps of single HIV-1 infection. Viruses 10, 275. https://doi.org/10.3390/v10050275.
Frank, J., 1995. Approaches to large-scale structures. Curr. Opin. Struct. Biol. 5, 194–201.
Fridmann-Sirkis, Y., Milrot, E., Mutsafi, Y., Ben-Dor, S., Levin, Y., Savidor, A., Kartvelishvily, E., Minsky, A., 2016. Efficiency in complexity: composition and dynamic nature of mimivirus replication factories. J. Virol. 90, 10039–10047.
Galas, L., Gallavardin, T., Bénard, M., Lehner, A., Schapman, D., Lebon, A., Komuro, H., Lerouge, P., Leleu, S., Franck, X., 2018. Probe, sample and instrument (PSI): the hat-trick for fluorescence live cell imaging. Chemosensors 6, 21.

García-Serradilla, M., Risco, C., Pacheco, B., 2019. Drug repurposing for new, efficient, broad spectrum antivirals. Virus Res. 264, 22–31.
Gelderblom, H.R., Hausmann, E.H., Ozel, M., Pauli, G., Koch, M.A., 1987. Fine structure of human immunodeficiency virus (HIV) and immunolocalization of structural proteins. Virology 156, 171–176.
Gershon, A.A., Sherman, D.L., Zhu, Z., Gabel, C.A., Ambron, R.T., Gershon, M.D., 1994. Intracellular transport of newly synthesized varicella-zoster virus: final envelopment in the trans-Golgi network. J. Virol. 68, 6372–6390.
Gillespie, L.K., Hoenen, A., Morgan, G., Mackenzie, J.M., 2010. The endoplasmic reticulum provides the membrane platform for biogenesis of the flavivirus replication complex. J. Virol. 84, 10438–10447.
Gómez-Aix, C., García-García, M., Aranda, M.A., Sánchez-Pina, M.A., 2015. Melon necrotic spot virus replication occurs in association with altered mitocondria. Mol. Plant Microbe Interact. 28, 387–397.
Grabenbauer, M., Geerts, W.J., Fernández-Rodríguez, J., Hoenger, A., Koster, A.J., Nilsson, T., 2005. Correlative microscopy and electron tomography of GFP through photooxidation. Nat. Methods 2, 857–862.
Griffith, G., Brands, R., Burke, B., Louvard, D., Warren, G., 1982. Viral membrane proteins acquire galactose in trans Golgi cisternae during intracellular transport. J. Cell Biol. 95, 781–792.
Hagemeijer, M.C., Verheije, M.H., Ulasli, M., Shaltiël, I.A., de Vries, L.A., Reggiori, F., Rottier, P.J.M., de Haan, C.A.M., 2010. Dynamics of coronavirus replication-transcription complexes. J. Virol. 84, 2134–2149.
Hagen, C., Grünewald, K., 2008. Microcarriers for high-pressure freezing and cryosectioning of adherent cells. J. Microsc. 230, 288–296.
Hagen, C., Dent, K.C., Zeev-Ben-Mordehai, T., Grange, M., Bosse, J.B., Whittle, C., Klupp, B.G., Siebert, C.A., Vasishtan, D., Bäuerlein, F.J., Cheleski, J., Werner, S., Guttmann, P., Rehbein, S., Henzler, K., Demmerle, J., Adler, B., Koszinowski, U., Schermelleh, L., Schneider, G., Enquist, L.W., Plitzko, J.M., Mettenleiter, T.C., Grünewald, K., 2015. Structural basis of vesicle formation at the inner nuclear membrane. Cell 163, 1692–1701.
Hanne, J., Zila, V., Heilemann, M., Müller, B., Kräusslich, H.-G., 2016. Super-resolved insights into human immunodeficiency virus biology. FEBS Lett. 590, 1858–1876.
Harak, C., Lohmann, V., 2015. Ultrastructure of the replication sites of positive-strand RNA viruses. Virology 479-480, 418–433.
Harris, K.M., Perry, E., Bourne, J., Feinberg, M., Ostroff, L., Hurlburt, J., 2006. Uniform serial sectioning for transmission electron microscopy. J. Neurosci. 26, 12101–12103.
Hayles, M.F., de Winter, D.A., Schneijdenberg, C.T., Meeldijk, J.D., Luecken, U., Persoon, H., de Water, J., de Jong, F., Humbel, B.M., Verkleij, A.J., 2010. The making of frozen-hydrated, vitreous lamellas from cells for cryo-electron microscopy. J. Struct. Biol. 172, 180–190.
Heiligenstein, X., Heiligenstein, J., Delevoye, C., Hurbain, I., Bardin, S., Paul-Gilloteaux, P., Sengmanivong, L., Régnier, G., Salamero, J., Antony, C., Raposo, G., 2014. The CryoCapsule: simplifying correlative light to electron microscopy. Traffic 15, 700–716.
Hellström, K., Vihinen, H., Kallio, K., Jokitalo, E., Ahola, T., 2015. Correlative light and electron microscopy enables viral replication studies at the ultrastructural level. Methods 90, 49–56.
Herpers, B., Xanthakis, D., Rabouille, C., 2010. ISH-IEM: a sensitive method to detect endogenous mRNAs at the ultrastructural level. Nat. Protoc. 5, 678–687.
Hillier, J., 1950. Electron microscopy of microorganisms and viruses. Annu. Rev. Microbiol. 4, 1–20.

Hinners, I., Moschner, J., Nolte, N., Hille-Rehfeld, A., 1999. The orientation of membrane proteins determined in situ by immunofluorescence staining. Anal. Biochem. 276, 1–7.
Hoppe, W., Gassmann, J., Hunsmann, N., Schramm, H.J., Sturm, M., 1974. Three-dimensional reconstruction of individual negatively stained yeast fatty-acid synthetase molecules from tilt series in the electron microscope. Hoppe Seylers Z. Physiol. Chem. 355, 1483–1487.
Hurbain, I., Sachse, M., 2011. The future is cold: cryo-preparation methods for transmission electron microscopy of cells. Biol. Cell 103, 405–420.
Ibiricu, I., Huiskonen, J.T., Döhner, K., Bradke, F., Sodeik, B., Grünewald, K., 2011. Cryo electron tomography of herpes simplex virus during axonal transport and secondary envelopment in primary neurons. PLoS Pathog. 7, e1002406.
Icha, J., Weber, M., Waters, J.C., Norden, C., 2017. Phototoxicity in live fluorescence microscopy, and how to avoid it. Bioessays 39 (8), 1700003.
Jackson, W.T., Giddings Jr., T.H., Taylor, M.P., Mulinyawe, S., Ravinovitch, M., Kopito, R.R., Kirkegaard, K., 2005. Subversion of cellular autophagosomal machinery by RNA viruses. PLoS Biol. 3 (5) e156.
Jouvenet, N., Bieniasz, P.D., Simon, S.M., 2008. Imaging the biogenesis of individual HIV-1 virions in live cells. Nature 454, 236–240.
Kajitani, N., Satsuka, A., Yoshida, S., Sakai, H., 2013. HPV18 E1^E4 is assembled into aggresome-like compartment and involved in sequestration of viral oncoproteins. Front. Microbiol. 4 (251), 1–11.
Kallio, K., Hellström, K., Balistreri, G., Jokitalo, E., Ahola, T., 2013. Template RNA length determines the size of replication complex spherules for Semliki Forest Virus. J. Virol. 87, 9125–9134.
Kanno, H., Speedy, R.J., Angell, C.A., 1975. Supercooling of water to −92°C under pressure. Science 189, 880–881.
Karreman, M.A., Mercier, L., Schieber, N.L., Shibue, T., Schwab, Y., Goetz, J.G., 2014. Correlating intravital multi-photon microscopy to 3D electron microscopy of invading tumor cells using anatomical reference points. PLoS One 9, e114448. https://doi.org/10.1371/journal.pone.0114448. eCollection 2014.
Kellenberger, E., 1991. The potential of cryofixation and freeze substitution: observations and theoretical considerations. J. Microsc. 161, 183–203.
Knoops, K., Kikkert, M., Worm, S.H., Zevenhoven-Dobbe, J.C., van der Meer, Y., Koster, A.J., Mommaas, A.M., Snijder, E.J., 2008. SARS-coronavirus replication is supported by a reticulovesicular network of modified endoplasmic reticulum. PLoS Biol. 6, e226.
Kopek, B.G., Perkins, G., Miller, D.J., Ellisman, M.H., Ahlquist, P., 2007. Three-dimensional analysis of a viral RNA replication complex reveals a virus-induced mini-organelle. PLoS Biol. 5, e220.
Kukulski, W., Schorb, M., Welsch, S., Picco, A., Kaksonen, M., Briggs, J.A., 2011. Correlated fluorescence and 3D electron microscopy with high sensitivity and spatial precision. J. Cell Biol. 192, 111–119.
Lee, J.-Y., Marshall, J.A., Bowden, D.S., 1994. Characterization of Rubella virus replication complexes using antibodies to double-stranded RNA. Virology 200, 307–312.
Lepault, J., Booy, F.P., Dubochet, J., 1983. Electron microscopy of frozen biological suspensions. J. Microsc. 129, 89–102.
Limpens, R.W., van der Schaar, H.M., Kumar, D., Koster, A.J., Snijder, E.J., van Kuppeveld, F.J., Bárcena, M., 2011. The transformation of enterovirus replication structures: a three-dimensional study of single- and double-membrane compartments. mBio 2, e00166-11.
López-Montero, N., Risco, C., 2011. Self-protection and survival of arbovirus-infected mosquito cells. Cell. Microbiol. 13, 300–315.

Lowen, R.G., Bocan, T.M., Kane, C.D., Cazares, L.H., Kota, K.P., Ladner, J.T., Nasar, F., Pitt, L., Smith, D.R., Sloveva, V., Sun, M.G., Zeng, X., Bavari, S., 2018. Countering Zika virus: the USAMRIID response. Adv. Exp. Med. Biol. 1062, 303–318.

Lucas, M.S., Günthert, M., Gasser, P., Lucas, F., Wepf, R., 2012. Bridging microscopes: 3D correlative light and scanning electron microscopy of complex biological structures. In: -Müller-Reichert, T., Verkade, P. (Eds.), Correlative Light and Electron Microscopy. In: Methods in Cell biology, 111, pp. 325–356.

Luther, P.K., Lawrence, M.C., Crowther, R.A., 1988. A method for monitoring the collapse of plastic sections as a function of electron dose. Ultramicroscopy 24, 7–18.

Madela, K., Banhart, S., Zimmermann, A., Piesker, J., Bannert, N., Laue, M., 2014. A simple procedure to analyze positions of interest in infectious cell cultures by correlative light and electron microscopy. In: Müller-Reichert, T., Verkade, P. (Eds.), Correlative Light and Electron Microscopy II. Methods in Cell biology, 124, pp. 93–110.

Magidson, V., Khodjakov, A., 2013. Circumventing photodamage in live-cell microscopy. Methods Cell Biol. 114, 545–560.

Magliano, D., Marshall, J.A., Bowden, D.S., Vardaxis, S., Meanger, J., Lee, J.Y., 1998. Rubella virus replication complexes are virus modified lysosomes. Virology 240, 57–63.

Martell, J.D., Deerinck, T.J., Sancak, Y., Poulos, T.L., Mootha, V.K., Sosinsky, G.E., Ellisman, M.H., Ting, A.Y., 2012. Engineered ascorbate peroxidase as a genetically encoded reporter for electron microscopy. Nat. Biotechnol. 30, 1143–1148.

Martínez, M.G., Snapp, E.-L., Perumal, G.S., Macaluso, F.P., Kielian, M., 2014. Imaging the alphavirus exit pathway. J. Virol. 88, 6922–6933.

Mastronarde, D.N., 1997. Dual-axis tomography: an approach with alignment methods that preserve resolution. J. Struct. Biol. 120, 343–352.

Mateer, E., Paessler, S., Huang, C., 2019. Confocal imaging of double-stranded RNA and pattern recognition receptors in negative-sense RNA virus infection. J. Vis. Exp. 143, e59095.

Mayhew, T., 2005. How to count your gold: a tutorial on TEM immunogold label quantification. Microsc. Anal. 12, 9–12.

McDonald, K., 2007. Cryopreparation methods for electron microscopy of selected model systems. In: McIntosh, J.R. (Ed.), Cellular Electron microscopy. In: Methods in Cell Biology, 79, pp. 23–56.

McDowall, A.W., Chang, J.J., Freeman, R., Lepault, J., Walte, R.C.A., Dubochet, J., 1983. Electron microscopy of frozen hydrated sections of vitreous ice and vitrified biological samples. J. Microsc. 131, 1–9.

Melia, C.E., van der Schaar, H.M., de Jong, A.W.M., Lyoo, H.R., Snijder, E.J., Koster, A.J., van Kuppeveld, F.J.M., Bárcena, M., 2018. The origin, dynamic morphology, and PI4P-independent formation of encephalomyocarditis virus replication organelles. mBio 9 e00420-18.

Mercogliano, C.P., DeRosier, D.J., 2006. Gold nanocluster formation using metallothionein: mass spectrometry and electron microscopy. J. Mol. Biol. 355, 211–223.

Mercogliano, C.P., DeRosier, D.J., 2007. Concatenated metallothionein as a clonable gold label for electron microscopy. J. Struct. Biol. 160, 70–82.

Milrot, E., Mutsafi, Y., Fridmann-Sirkis, Y., Shimoni, E., Rechav, K., Gurnon, J.R., Van Etten, J.L., Minsky, A., 2016. Virus-host interactions: insights from the replication cycle of the large *Paramecium bursaria chlorella virus*. Cell. Microbiol. 18, 3–16.

Möbius, W., Posthuma, G., 2019. Sugar and ice: immunoelectron microscopy using cryosections according to the Tokuyasu method. Tissue Cell 57, 90–102. pii: S0040-8166(18)30214-3. https://doi.org/10.1016/j.tice.2018.08.010.

Monaghan, P., Cook, H., Hawes, P., Simpson, J., Tomley, F., 2003. High-pressure freezing in the study of animal pathogens. J. Microsc. 212, 62–70.

Morphew, M.K., O'Toole, E.T., Page, C.L., Pagratis, M., Meehl, J., Giddings, T., Gardner, J.M., Ackerson, C., Jaspersen, S.L., Winey, M., Hoenger, A., McIntosh, J.R., 2015. Metallothionein as a clonable tag for protein localization by electron microscopy of cells. J. Microsc. 260, 20–29.
Moss, B., 2015. Poxvirus membrane biogenesis. Virology 479-480, 619–626.
Müller-Reichert, T., Verkade, P., 2012. Correlative light and electron microscopy. Methods in Cell Biology, 111, Elsevier.
Müller-Reichert, T., Verkade, P., 2014. Correlative light and electron microscopy II. Methods in Cell Biology, 124, Elsevier.
Mutsafi, Y., Zauberman, N., Sabanay, I., Minsky, A., 2010. Vaccinia-like cytoplasmic replication of the giant mimivirus. Proc. Natl. Acad. Sci. U. S. A. 107, 5978–5982.
Mutsafi, Y., Shimoni, E., Shimon, A., Minsky, A., 2013. Membrane assembly during the infection cycle of the giant Mimivirus. PLoS Pathog. 9 e1003367.
Mutsafi, Y., Fridmann-Sirkis, Y., Milrot, E., Hevroni, L., Minsky, A., 2014. Infection cycles of large DNA viruses: emerging themes and underlying questions. Virology 466-467, 3–14.
Novoa, R.R., Calderita, G., Arranz, R., Fontana, J., Granzow, H., Risco, C., 2005. Virus factories: associations of cell organelles for viral replication and morphogenesis. Biol. Cell 97, 147–172.
Oorschot, V.M., Sztal, T.E., Bryson-Richardson, R.J., Ramm, G., 2014. Immuno correlative light and electron microscopy on Tokuyasu cryosections. 2014, In: Müller-Reichert, T., Verkade, P. (Eds.), Correlative Light and Electron Microscopy II. Methods Cell Biol, 124, pp. 241–258.
Paul, D., Hoppe, S., Saher, G., Krijnse-Locker, J., Bartenschlager, R., 2013. Morphological and biochemical characterization of the membranous hepatitis C virus replication compartment. J. Virol. 87, 10612–10627.
Pelchen-Matthews, A., Marsh, M., 2007. Electron microscopy analysis of viral morphogenesis. Methods Cell Biol. 79, 515–542.
Penttila, A., Kalimo, H., Trump, B.F., 1974. Influence of glutaraldehyde and/or osmium tetroxide on cell volume, ion content, mechanical stability, and membrane permeability of Ehrlich ascites tumor cells. J. Cell Biol. 63, 197–214.
Rhim, J.S., Jordan, L.E., Mayor, H.D., 1962. Cytochemical, fluorescent-antibody and electron microscopic studies on the growth of reovirus (ECHO 10) in tissue culture. Virology 17, 342–355.
Riehle, U., Hoechli, M., 1973. The theory and technique of highpressure freezing. In: Benedetti, E.L., Favard, P. (Eds.), Freeze-Etching Technique and Application. Société Francaise de Microscopie Électronique, pp. 31–61.
Risco, C., Sanmartín-Conesa, E., Tzeng, W.P., Frey, T.K., Seybold, V., de Groot, R.J., 2012. Specific, sensitive, high-resolution detection of protein molecules in eukaryotic cells using metal-tagging transmission electron microscopy. Structure 20, 759–766.
Risco, C., Fernández de Castro, I., Sanz-Sánchez, L., Narayan, K., Grandinetti, G., Subramaniam, S., 2014. Three-dimensional imaging of viral infections Annu. Rev. Virol. 1, 453–473.
Romero-Brey, I., Bartenschlager, R., 2014. Membranous replication factories induced by plus-strand RNA viruses. Viruses 6, 2826–2857.
Romero-Brey, I., Merz, A., Chiramel, A., Lee, J.Y., Chlanda, P., Haselman, U., Santarella-Mellwig, R., Habermann, A., Hoppe, S., Kallis, S., Antony, C., Krijnse-Locker, J., Bartenschlager, R., 2012. Three-dimensional architecture and biogenesis of membrane structures associated with hepatitis C virus replication. PLoS Pathog. 8 (12), e1003056.
Sabatini, D.D., Bensch, K., Barnett, R.J., 1963. Cytochemistry and electron microscopy. The preservation of cellular ultrastructure and enzymatic activity by aldehyde fixation. J. Cell Biol. 17, 19–58.

Sachse, M., Fernández de Castro, I., Fournier, G., Naffakh, N., Risco, C., 2018. Metal-tagging electron microscopy and immunogold labeling on Tokuyasu cryosections to image influenza A virus ribonucleoprotein transport and packaging. Methods Mol. Biol. 1836, pp. 281–301, Springer.

Salmons, T., Kuhn, A., Wylie, F., Schleich, S., Rodríguez, J.R., Rodríguez, D., Esteban, M., Griffiths, G., Krijnse Locker, J., 1997. Vaccinia virus membrane proteins p8 and p16 are cotranslationally inserted into the rough endoplasmic reticulum and retained in the intermediate compartment. J. Virol. 71, 7404–7420.

Santarella-Mellwig, R., Haselmann, U., Schieber, N.L., Walther, P., Schwab, Y., Antony, C., Bartenschlager, R., Romero-Brey, I., 2018. Correlative light electron microscopy (CLEM) for tracking and imaging viral protein associated structures in cryo-immobilized cells. J. Vis. Exp. 2018, 139. https://doi.org/10.3791/58154.

Scaturro, P., Cortese, M., Chatel-Chaix, L., Fischk, W., Bartenschlager, R., 2015. Dengue virus non-structural protein 1 modulates infectious particle production via interaction with the structural proteins. PLoS Pathog. 11, e1005277.

Schramm, B., de Haan, C.A.M., Young, J., Doglio, L., Schleich, S., Reese, C., Popov, A.V., Steffen, W., Schroer, T., Krijnse Locker, J., 2006. Vaccinia-virus-induced cellular contractility facilitates the subcellular localization of the viral replication sites. Traffic 7, 1352–1367.

Schwarz, H., Humbel, B.M., 2014. Correlative light and electron microscopy using immunolabeled sections. In: Kuo, J. (Ed.), Electron Microscopy. Methods Mol Biol, 1117, pp. 559–592.

Shi, X., van Mierlo, J.T., French, A., Elliott, R.M., 2010. Visualizing the replication cycle of Bunyamwera orthobunyavirus expressing fluorescent protein-tagged Gc glycoprotein. J. Virol. 84, 8460–9469.

Singer, S.J., Schick, A.F., 1961. The properties of specific stains for electron microscopy prepared by the conjugation of antibody molecules with ferritin. J. Biophys. Biochem. Cytol. 9, 519–537.

Slot, J.W., Geuze, H.J., 1981. Sizing of protein A-colloidal gold probes for immunoelectron microscopy. J. Cell Biol. 90, 533–536.

Sosinsky, G.E., Crum, J., Jone, S.Y.Z., Lanman, J., Smarr, B., Terada, M., Martone, M.E., Deerinck, T.J., Johnson, J.E., Ellisman, M.H., 2008. The combination of chemical fixation procedures with high pressure freezing and freeze substitution preserves highly labile tissue ultrastructure for electron tomography applications. J. Struct. Biol. 161, 359–371.

Spuul, P., Balistreri, G., Kääriäinen, L., Ahola, T., 2010. Phosphatidylinositol 3-kinase-, actin-, and microtubule-dependent transport of Semliki Forest Virus replication complexes from the plasma membrane to modified lysosomes. J. Virol. 84, 7543–7557.

Spuul, P., Balistreri, G., Hellström, K., Golubtsov, A.V., Jokitalo, E., Ahola, T., 2011. Assembly of alphavirus replication complexes from RNA and protein components in a novel trans-replication system in mammalian cells. J. Virol. 85, 4739–4751.

Suárez, C., Welsch, S., Chlanda, P., Hagen, W., Hoppe, S., Kolovou, A., Pagnier, I., Raoult, D., Krijnse Locker, J., 2013. Open membranes are the precursors for assembly of large DNA viruses. Cell. Microbiol. 15, 1883–1895.

Tenorio, R., Fernández de Castro, I., Knowlton, J.J., Zamora, P.F., Lee, C.H., Mainou, B.A., Dermody, T.S., Risco, C., 2018. Reovirus σNS and μNS proteins remodel the endoplasmic reticulum to build replication neo-organelles. mBio 9, e01253-18.

Titze, B., Genoud, C., 2016. Volume scanning electron microscopy for imaging biological ultrastructure. Biol. Cell 108, 307–323.

Tokuyasu, K.T., 1973. A technique for ultracryotomy of cell suspensions and tissues. J. Cell Biol. 57, 551–565.

Tolonen, N., Doglio, L., Schleich, S., Krijnse Locker, J., 2001. Vaccinia virus DNA replication occurs in endoplasmic reticulum-enclosed cytoplasmic mini-nuclei. Mol. Biol. Cell 12, 2031–2046.

Van der Schaar, H.M., Melia, C.E., van Bruggen, J.A.C., Strating, J.R.P.M., van Geenen, M.E.D., Koster, A.J., Bárcena, M., van Kuppeveld, F.J.M., 2016. Illuminating the sites of enterovirus replication in living cells by using a split-GFP-tagged viral protein. mSphere 1 (4), e00104-16.

Verkade, P., 2008. Moving EM: the rapid transfer system as a new tool for correlative light and electron microscopy and high throughput for high-pressure freezing. J. Microsc. 230, 317–328.

Villinger, C., Neusser, G., Kranz, C., Walther, P., Mertens, T., 2015. 3D analysis of HCMV induced-nuclear membrane structures by FIB/SEM tomography: insight into an unprecedented membrane morphology. Viruses 7, 5686–5704.

Wan, J., Basu, K., Miu, J., Vali, H., Zheng, H., Laliberté, J.-F., 2015. Ultrastructural characterization of turnip mosaic virus-induced celular rearrangements reveals membrane-bound viral particles accumulating in vacuoles. J. Virol. 89, 12441–12456.

Welsch, S., Miller, S., Romero-Brey, I., Merz, A., Bleck, C.K.E., Walther, P., Fuller, S.D., Antony, C., Krijnse-Locker, J., Bartenschlager, R., 2009. Composition and three-dimensional architecture of the Dengue virus replication and assembly sites. Cell Host Microbe 5, 365–375.

Westaway, E.G., Khromykh, A.A., Mackenzie, J.M., 1999. Nascent flavivirus RNA colocalized in situ with double-stranded RNA in stable replication complexes. Virology 258, 108–117.

White, D.L., Andrews, S.B., Faller, J.W., Barrnett, R.J., 1976. The chemical nature of osmium tetroxide fixation and staining of membranes by x-ray photoelectron spectroscopy. Biochim. Biophys. Acta 436, 577–592.

Wileman, T., 2007. Aggresomes and pericentriolar sites of virus assembly: cellular defense or viral design? Annu. Rev. Microbiol. 61, 7905–7912.

Witte, R., Andriasyan, V., Georgi, F., Yakimovich, A., Greber, U.F., 2018. Concepts in light microscopy of viruses. Viruses 10, 202. https://doi.org/10.3390/v10040202.

Wolff, G., Hagen, C., Grünewald, K., Kaufmann, R., 2016. Towards correlative super-resolution fluorescence and electron cryo-microscopy. Biol. Cell 108, 245–258.

Wölk, B., Büchele, B., Moradpour, D., Rice, C.M., 2008. A dynamic view of hepatitis C virus replication complexes. J. Virol. 82, 10519–10531.

Yakushevska, A.E., Lebbink, M.N., Geerts, W.J., Spek, L., van Donselaar, E.G., Jansen, K.A., Humbel, B.M., Post, J.A., Verkleij, A.J., Koster, A.J., 2007. STEM tomography in cell biology. J. Struct. Biol. 159, 381–391.